Available online at www.sciencedirect.com
ScienceDirect
Journal of Photochemistry and Photobiology A: Chemistry 191 (2007) 153–161
Journal of Photochemistry and Photobiology A:Chemistry
www.elsevier.com/locate/jphotochem

Synthesis and characterization of MnO_x/TiO_2 nanoparticles for photocatalytic oxidation of indigo carmine dye

Mohamed Mokhtar Mohamed [a,*,1], I. Othman [b], R.M. Mohamed [c]

[a] *Faculty of Science, Chemistry Department, Benha University, Benha, Egypt*
[b] *Faculty of Science, Chemistry Department, Al-Azhar University, Naser City, Cairo, Egypt*
[c] *Central Metallurgical R&D Institute, Department of Nanostructured Material, Helwan, Cairo, Egypt*

Received 6 January 2007; received in revised form 17 April 2007; accepted 18 April 2007
Available online 24 April 2007

Abstract

Manganese (10 wt.%) supported on titania synthesized by sol–gel (Mn/TiO_{2SG}) and impregnation ($Mn/TiO_{2D\text{-}imp}$) methods in addition to their precursors TiO_{2SG} and TiO_{2D} (Degussa) materials were characterized by measuring the surface texturing, Fourier transform infrared spectroscopy, X-ray diffraction, particle size (analyzer) and electrophoretic mobility (zeta potential). These materials were tested for adsorption and mineralization (in the presence of UV irradiation) of indigo carmine (IC) dye. Through comparison of the results, the photocatalytic degradation of $Mn/TiO_{2D\text{-}imp}$ indicated the highest activity (98%) comparatively. This was due to 34% of the support titania is covered by Mn species in $Mn/TiO_{2D\text{-}imp}$ mainly as Mn_2O_3 moieties, as validated from IR results (605, 714 cm^{-1}). On the other hand, Mn in Mn/TiO_{2SG} was incorporated in titania lattice mainly in tetrahedral coordination sites as β-MnO_2 (655, 693 cm^{-1}) and only exposes surface coverage comprises of 10%. The adsorption of IC dye onto TiO_{2D} was considerably higher (88%) than rest of materials due to increasing OH groups, large surface to volume ratio and moderate pore radius (33 Å) that was accessible to facile IC diffusion. TiO_{2SG} and Mn/TiO_{2SG} presented lower activity either in adsorption and photocatalysis compared with $Mn/TiO_{2D\text{-}imp}$. There is no apparent size effect on IC degradation over former catalysts since they have comparable values (48–43 nm). The influence of time on the decolorization rate of IC on $Mn/TiO_{2\text{-}Dimp}$ was thoroughly investigated and well pH regulated and correlated with ZPC of MnO_x species and surface properties.

Keywords: Dye mineralization; Mn/TiO_2; Impregnation; Sol–gel; Texturing; XRD; N_2 adsorption; Zeta potential

1. Introduction

Wastewater effluents in some industries, such as dyestuff, textiles, leather, paper, and plastics, contain several kinds of synthetic dyestuffs. A very small dye amount in water is highly visible and can be toxic to life and harmful to human beings. Hence, the removal of color from process or waste effluents becomes of fundamental importance to the environment [1,2].

Doping titania; of large band gap (3–3.2 eV) and very stable under illumination for H_2O photolysis and absorbs only UV part of the solar emission, with transition metal ions has been tested as a promising way of improving the photocatalytic activity of semiconductor oxides. The incorporation of metal ions into titania crystal lattice can significantly extend the absorption by the photocatalysts into visible range. The effect of doping is to change the equilibrium concentration of electrons or holes [3–5]. Previous studies on the phase transformation characteristics of doped TiO_2 have shown stabilization of both anatase and rutile phases for different experimental conditions [6].

MnO_2 was among the oldest examined metal oxide catalyst and found to possess a potential activity in redox reactions. Manganese oxide surface have been found to expose metal (Mn^{n+}), oxide (O^{2-}) and defect sites of various oxidation states, degrees of coordination unsaturation and, thus, acid and base properties. Furthermore, the d–d electron exchange interactions between intimately coupled manganese ions of different oxidation states [Mn^{n+}–O–$Mn^{(n+1)+}$] furnish the electron-mobile environment necessary for the surface redox activity [7]. The current search for candidate metal oxides for the chemical makeup of total

* Corresponding author. Tel.: +20 26073049.
E-mail address: mohmok2000@yahoo.com (M.M. Mohamed).
[1] On leave in Fac. Appl. Sci., Umm Al Qura Univ., Makka, Saudia Arabia.

1010-6030/$ – see front matter © 2007 Published by Elsevier B.V.
doi:10.1016/j.jphotochem.2007.04.017

oxidation (photo-degradation) catalysts for aromatic organics open up new application horizons for titania and manganese oxide based catalysts. Such mixed oxide can fulfils some terms of appropriateness such as, high thermal stability, tolerance to extended defect structures, reversible redox behavior and capability of oxygen activation. For examples, the work of Arroyo et al. [6] on manganese (Mn^{2+}) doped titania showed stabilization of the anatase phase for low doping levels, prior to segregation of the doping to the surface at higher concentration and stabilization of the rutile phase. It has been shown that manganese oxides are insoluble [8,9]. However, the amount of manganese dissolved in solution can be increased considerably in acidic medium with the addition of organic compounds such as dyes [10]. But the further adsorption and oxidation of dye compound on the mineral particles interface reduce their surface areas and lead to inhibition of the process [11]. Recently, Mn/TiO_2 has been examined as a catalyst for hydrogenation of methyl benzoate to benzaldehyde, low temperature selective catalytic reduction of NO with ammonia and ozonation of phenol [12–14]. Indigo carmine (IC) is one of the oldest dyes and still one of the most important used. Its major industrial application in dyeing of clothes (blue jeans) and other blue denim [15] has attracted many researchers to mineralize it utilizing different systems including TiO_2/UV, H_2O_2/UV, Ozone and Fenton reagent [16–19].

In this work, correlation between surface, crystallites size, photocatalytic behaviors and adsorption properties of Mn supported on TiO_2; either prepared by sol–gel or impregnation methods, were studied. Synthesizing Mn/TiO_2 catalysts using sol–gel is based on the importance of nanomaterial of different shapes in exhibiting new properties such as enhanced absorption and ultrafast electron-hole dynamics. The catalysts were characterized by N_2 adsorption, FTIR, XRD, zeta potential and particle size distribution. The removal of IC dye at room temperature in aqueous catalyst suspension was used as a test reaction in presence and absence of UV lamp.

2. Experimental

2.1. Materials

Titanium dioxide powder P-25, which is predominantly anatase, was purchased from Degussa (TiO_2-D-Germany) and was used without any further treatment. Manganese nitrate [$Mn(NO_3)_2$], Titanium (IV) isobutoxide and ethanol were delivered, respectively, from Merck and Fluka companies.

Indigo Carmine dye [3,3′-Dioxo-1,3,1′,3′-tetrahydro-[2,2′]-bi-indolylidene-5,5′-disulfonic acid disodium salt] was delivered from the general chemical company limited, Wembley Middlesex-England.

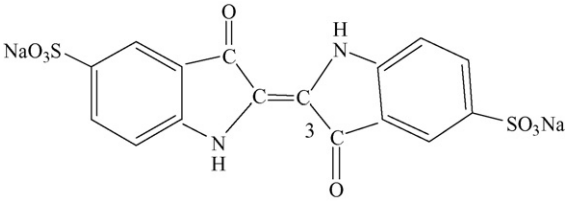

M.F. $C_{16}H_8N_2Na_2O_8S_2$, M. wt. 466.35 g/L. The peak intensity is at 608 nm; molar absorbtivity is 6309 mol^{-1} cm^{-1}.

2.1.1. Preparation of Mn/TiO_2

Titania sol–gel ($TiO_{2\text{-}SG}$) was prepared according to following molar ratios:

$$Ti(C_4H_9O_4): \quad 20C_2H_5OH: \quad 4H_2O: \quad 0.001HNO_3$$

$Ti(C_4H_9O_4)$ was first dissolved in ethanol medium to form a solution. The amounts of water and nitric acid were added drop wise into the sol followed by stirring for 30 min at room temperature. The prepared sols were left to stand for the formation of gel. After the gelation was completed, the gels were aged for 24 h at room temperature and then calcined at 550 °C for 6 h.

The sample prepared by impregnation ($Mn/TiO_{2D\text{-}imp}$) followed the sequence of adding an aqueous solution of $Mn(NO_3)_2$ on $TiO_{2\text{-}D}$; purchased from Degussa. The volume of solution used was necessary to completely wet sample. The reaction temperature was adapted at 80 °C for 4 h using temperature controller type (REX-P 90). The precursor sample was then dried at 110 °C overnight and calcined in air at 550 °C for 6 h.

In the case of manganese loaded titania prepared by sol–gel technique, $Mn(NO_3)_2$ solution was added to Ti(IV) isobutoxide at constant temperature (60 °C) using a water/solvent ratio of 4 in the gelation solution. The solids were dried at 120 °C for 12 h and calcined in air at 550 °C for 6 h. Mn loading was 10 wt.% in all the prepared samples. The solids were labeled as: $TiO_{2\text{-}D}$, $TiO_{2\text{-}SG}$, $Mn/TiO_{2D\text{-}imp}$ and $Mn/TiO_{2\text{-}SG}$ characterizing TiO_2 purchased from Degussa, TiO_2 prepared by sol–gel, Mn supported on titania support either prepared by impregnation and sol–gel, respectively.

2.2. Characterization techniques

The X-ray diffractograms of various titania samples were measured by using a Bruker axis, D8 advance. The patterns were run with Ni-filtered copper radiation ($\lambda = 1.5404$ Å) at 30 kV and 10 mA with a scanning speed of $2\theta = 2.5°$ min^{-1}. For phase identification purposes, automatic JCPDS library search and match was used.

FT-IR spectra were recorded at room temperature using JASCO FT-IR-40 apparatus, plus Japan in two ranges at 3800–3300 and 1000–450 cm^{-1} with a resolution of 2 cm^{-1} both on KBr pellet techniques.

Dry nitrogen was used as a purge gas at a rate of 30 ml/min. The nitrogen adsorption isotherms were measured at −196 °C using a conventional volumetric apparatus. The specific surface area was obtained using the BET method.

Dynamic light scattering, LB-500, was used for determining particles size. Sample preparation was carried out as follows: dispersion of 20 mg of the sample in H_2O together with sodium hexametaphosphate was stirred for 10 min. The suspension was ultrasonicated for 10 min then acquired for measurement.

Zeta potentials of suspension samples were measured at room temperature using a zeta meter 3.0 equipped with a microprocessor unit. The unit automatically calculates the electrophoretic mobility of the particle and converts the electrophoretic mobility

into zeta potential in terms of Smoluchowski equation. A 0.1 g amount of the solid sample was conditioned in 50 ml of 0.001 M NaCl solutions at various pH values for 24 h in a shaking bath. Before installing for measurements, the suspension was kept for 5 min to let the larger particles settle. Each data point is an average of approximately 20 measurements. The pH of the suspension was adjusted using dilute solutions of HCl and NaOH [13]. All solutions were prepared using bi-distilled water. The pH of the suspension was measured using a pH meter-Orion 920A.

2.3. Catalytic activity

2.3.1. IC dye adsorption

Adsorption experiments of IC on the prepared catalysts in the absence of ultraviolet irradiation were carried out in a batch mode. A 250 ml volume of the IC dye (100 ppm), previously adjusted to affix pH value with diluted NaOH and HCl solutions, was added to a 300 ml beaker containing different amounts of suspended catalysts. The suspensions were immediately shaken in an air for 1 h using a magnetic stirrer prior to following up the uptaken amounts of the dye by catalysts that were maintained for 1 h adsorption time.

2.3.2. Photocatalytic evaluation

All the experiments were carried out using a horizontal cylinder annular batch reactor. IC was selected as a model for the photocatalytic degradation experiments because it is a non-volatile and common contaminant in the industrial wastewaters. A black light-blue florescent bulb (F18W- BLB) was positioned at the axis of the reactor to supply UV illumination. The light intensity after passing through a reaction suspension was 365 nm. The experiments were performed by suspending calculated amount of the catalyst into IC solution (100 ppm). The reaction was carried out isothermally at 25 °C and samples of the reaction mixture were taken at time intervals for a total reaction time 1 h. The disappearance of IC was analyzed by UV–vis spectrophotometer (JASCO V-570 unit, serial No 29635) over the 190–800 nm range. Calibration plots based on Beer-Lamberts law were established relating the absorbance to the concentration. The decolorization was determined at the maximum 608 nm. % Removal efficiency of IC was measured by applying the following equation

$$\%\,\text{Removal efficiency} = \frac{(C_o - C)}{C_o \times 100}$$

where C_o is the original indigo carmine (IC) content and C is the retained IC in solution.

3. Results and discussion

3.1. XRD and crystallite size

The diffractograms of $TiO_{2\text{-}D}$, $Mn/TiO_{2\text{-}Dimp}$, $TiO_{2\text{-}SG}$, and $Mn/TiO_{2\text{-}SG}$ solids were displayed in Fig. 1. In all samples, the main diffraction line corresponds to anatase at $2\theta = 25.4^\circ$ giving interplanar distance of 3.52 Å. In $TiO_{2\text{-}SG}$ and $Mn/TiO_{2\text{-}SG}$,

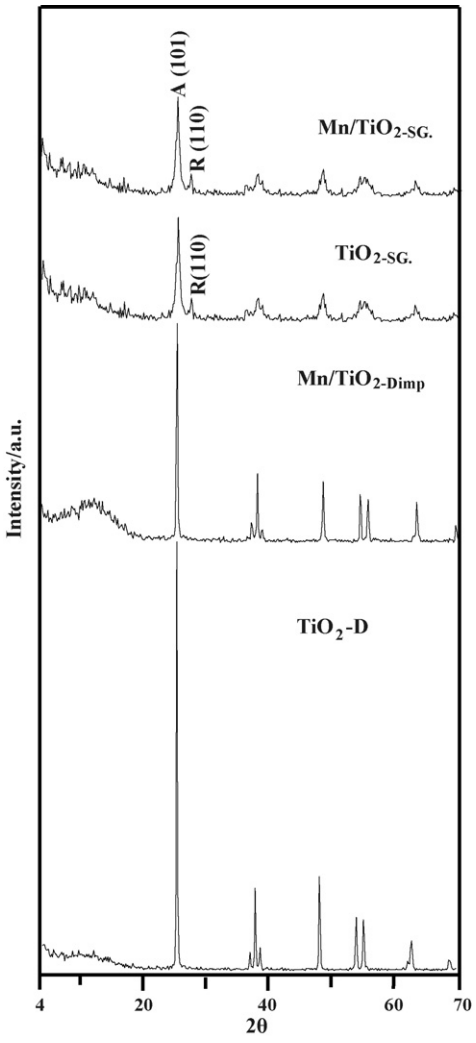

Fig. 1. XRD patterns of $TiO_{2\text{-}D}$, $Mn/TiO_{2D\text{-}imp}$, $TiO_{2\text{-}SG}$ and $Mn/TiO_{2\text{-}SG}$.

small lines for rutile at $2\theta = 27.46^\circ$ correspond to $d = 3.245$ Å were depicted. The latter samples affirmed that the anatase phase was the major phase representing ~90%. The absence of rutile phase in $TiO_{2\text{-}D}$ could be due to the poor contact between two phases and to the extremely small size. Table 1 compiles the anatase extent in the prepared solids. The higher proportion of the anatase contributed in $TiO_{2\text{-}D}$ is attained due to the high proportion of surface OH groups [20]. However, the insertion of Mn in titania lattice decreases this proportion suggesting the interaction of Mn with surface OH groups of titania. The $Mn/TiO_{2\text{-}Dimp}$ and $Mn/TiO_{2\text{-}SG}$ samples did not exhibit any line for Mn species indicating their dispersion and/or incorporation inside titania lattice. The latter samples exhibit broad lines characteristic of small crystallites size.

Inclusion of Mn in the matrix of supported system resulted in measurable degree of crystallinity and crystallite size of the phases present. For the sample $TiO_{2\text{-}D}$, the crystallite size of anatase phase, which was used as a measure of TiO_2 crystallinity, decreases when impregnated with Mn, from 65 to 58 nm (Table 1) However, for $TiO_{2\text{-}SG}$, the initial anatase crystallite size decreased only slightly from 48 to 43 nm in $Mn/TiO_{2\text{-}SG}$ It can be

Table 1
Crystallites size, crystallinity and lattice parameters of various TiO_2 and Mn/TiO_2 materials prepared by different methods

Samples	Crystallites size determined by Scherrer Eq. D (nm)		X_r	Crystallinity of anatase %	Mean particle size (nm)	Lattice parameter (Å)	
	A	R				a	c
$TiO_{2\text{-D}}$	65	0	–	100	80	3.790	9.503
$Mn/TiO_{2D\text{-imp}}$	58	0	–	58	75	3.791	9.560
$TiO_{2\text{-SG.}}$	48	51	0.056	25	60	3.792	9.504
Mn/TiO_{2SG}	43	55	0.184	25	55	3.793	9.489

X_r, the mass fraction of rutile was determined by the following Eq.: $X_{rutile} = 1/1 + k\,(I_a + I_r)$ where I_a and I_r are integrated peak intensities of anatase and rutile peaks, respectively. The empirical constant k was determined via an XRD analysis of powders of known proportions of pure anatase and pure rutile and equal 0.79. Mean particle size is determined by using particle size analyzer. Crystallinity of anatase % is calculated by integrated intensities of anatase (1 0 1) peak. D (nm) is crystallites size determined by Scherrer equation. Lattice parameter of anatase TiO_2.

suggested that the reduction process of nanocrystalline anatase is mainly because of dispersing the single crystals within the agglomerates, and finally the original agglomerate transforms to a smaller single crystal [21]. The particles size, determined by particle size analyzer (Fig. 2; Table 1), exhibited an increase comprised of 23–29% when compared with crystallites size determined by Scherrer equation enclosing that the crystallites are not of uniform size, but rather some type of distribution [22]. These results indicate that individual particles may contain crystals other than anatase or domains having different orientations [23]. Table 1 also shows that the lattice parameter a of TiO_2 anatase does not change in comparison to the JCPDS value but the c value shows an enhancement in $Mn/TiO_{2\text{-Dimp}}$ where it becomes smaller in $Mn/TiO_{2\text{-SG}}$ suggesting incorporation of Mn in the former and displacements of atoms from ideal sites in the latter [24].

3.2. Surface texturing

Specific surface area of $TiO_{2\text{-D}}$ is reduced by 12.7% when impregnated with Mn ions ($Mn/TiO_{2\text{-Dimp}}$) and exhibited a decrease in pore volume comprised of 5.5% with slight changes in pore radius from 33 to 35 Å. This point to deposition of Mn ions inside some pores specifically those of microporous characters as emphasized in Table 2 that showed a decrease in microporous volume and surface from 0.287 to 0.278 cm^3/g and from 217 to 199 m^2/g, respectively. A decrease in external surface area following Mn insertion from 41 to 36 m^2/g was also depicted enclosing the presence of residual Mn species on the external surface of titania. Increasing the surface area of $Mn/TiO_{2\text{-SG}}$ than $TiO_{2\text{-SG}}$ by 24.4% is attributed to that Mn ions provide additional nucleation sites, which lead to a solid

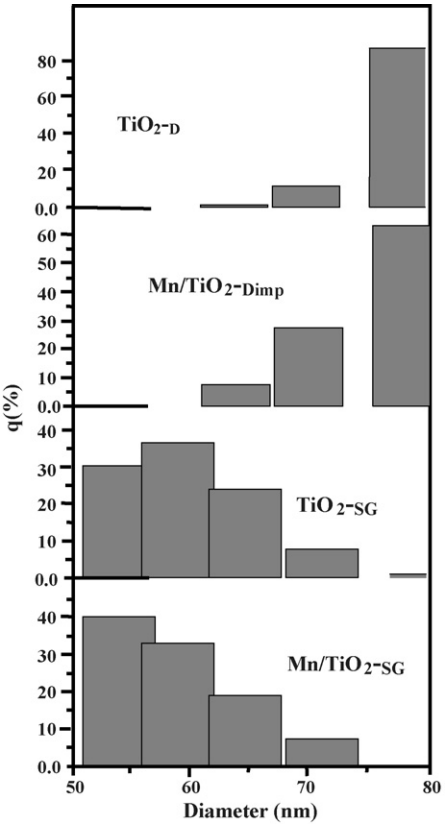

Fig. 2. Particle size distribution of $TiO_{2\text{-D}}$, $Mn/TiO_{2D\text{-imp}}$, $TiO_{2\text{-SG}}$ and $Mn/TiO_{2\text{-SG}}$.

with higher surface area [25]. Fig. 3 shows that all samples furnished upward deviations illustrating the presence of mesopores as r occurs in the range 27–46 Å. The upward deviation of

Table 2
Texture parameters of variousTiO_2 and Mn/TiO_2 materials prepared by different methods

Sample	S_{BET}(m^2/g)	S_t (m^2/g)	V_p^{total} (cm^3/g)	r^- (Å)	S^{μ} (m^2/g)	S^{ext}(m^2/g)	S^{wid} (m^2/g)	V_p^{μ} (cm^3/g)	V_p^{wid} (cm^3/g)	Microporosity %	C-const
$TiO_{2\text{-D}}$	283	286	0.3673	33	217	41	61	0.287	0.0803	85	14
$Mn/TiO_{2\text{-imp}}$	247	231	0.3470	35	199	36	49	0.278	0.0690	87	15
$TiO_{2\text{-SG}}$	221	218	0.4024	46	169	44	50	0.310	0.0924	86	30
$Mn/TiO_{2\text{-SG}}$	275	263	0.2939	27	218	30	55	0.235	0.0589	92	17

Note: Bet-surface area (S_{BET}), Total pore volume (V_p), Mean pore radius (r^-), Surface area derived from V_{l-t} plots (S_t), surface area of micropores (S^{μ}), External surface area (S^{ext}), surface area of wide pores (S^{wid}), volume of micropores V_p^{μ}, volume of wide pores (V_p^{wid}) and microporosity percentages $V_p^{mic}/V_p^{total} \times 100$.

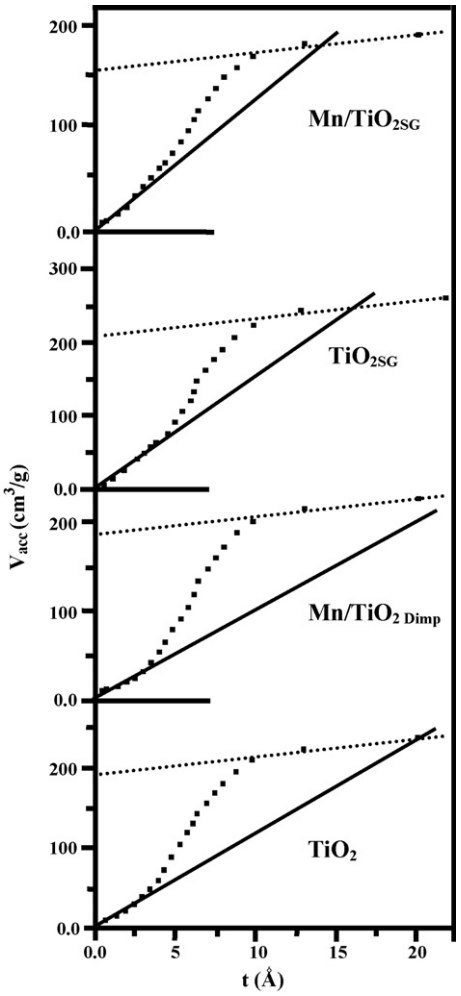

Fig. 3. $V_{l\text{-}t}$ plots of $TiO_{2\text{-}D}$, $Mn/TiO_{2D\text{-}imp}$, $TiO_{2\text{-}SG}$ and $Mn/TiO_{2\text{-}SG}$.

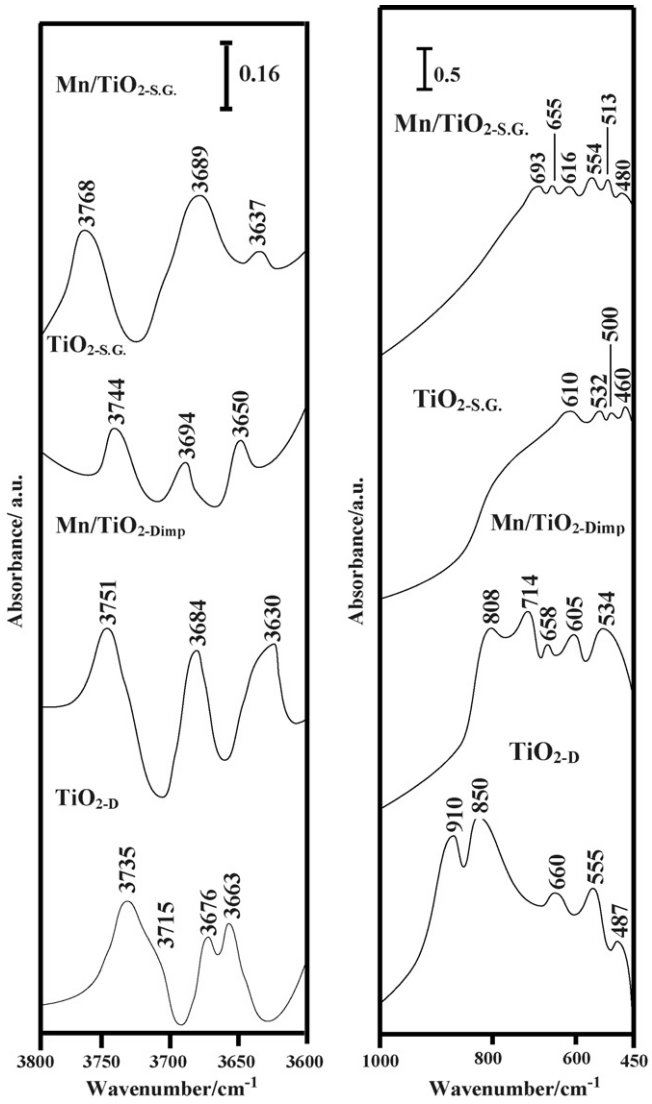

Fig. 4. FTIR spectra of $TiO_{2\text{-}D}$, $Mn/TiO_{2\text{-}Dimp}$, $TiO_{2\text{-}SG}$ and $Mn/TiO_{2\text{-}SG}$ in the low frequency region (450–1300 cm^{-1}) and high OH groups region (3600–4000 cm^{-1}).

$Mn/TiO_{2\text{-}Dimp}$ presented larger swing than that of $TiO_{2\text{-}D}$ reflecting the enforced location of some Mn ions inside titania pores causing enlargement. Conversely, $Mn/TiO_{2\text{-}SG}$ indicated smaller swing than that of $TiO_{2\text{-}SG}$ implicating the blockage of some titania pores by Mn ions. The insertion of Mn inside titania lattice was mainly deposited in wide pores that by its turn transferred to narrower ones as a result of decreasing the pore radius from 46 to 27 Å and pore volume from 0.4024 to 0.2939 cm^3/g. This definitely explains increasing the surface area of $Mn/TiO_{2\text{-}SG}$ than $TiO_{2\text{-}SG}$ by 24.4%.

3.3. FTIR spectroscopy

The FTIR spectra of $TiO_{2\text{-}D}$, $Mn/TiO_{2\text{-}Dimp}$, $TiO_{2\text{-}SG}$ and $Mn/TiO_{2\text{-}SG}$ samples are depicted in Fig. 4. The spectrum of $TiO_{2\text{-}D}$ exhibits strong absorption bands at 487 and 555 cm^{-1} due to the vibrations of Ti–O–Ti and Ti–O bonds, respectively, in the TiO_2 lattice [26,27]. The bands centered at 850 and 910 cm^{-1} may be assigned to characteristics O–O stretching vibration of peroxo groups, thus the band observed at 660 cm^{-1} may have been due to the vibration of the Ti–O–O bond [27].

The Spectrum of $Mn/TiO_{2\text{-}Dimp}$ shows the appearance of new bands at 605 and 714 cm^{-1} those were absent in the parent $TiO_{2\text{-}D}$ thus, it is reasonable to associate them with Mn–O vibrations and specifically to lattice vibrations of Mn^{III}–O bonds in Mn_2O_3 moieties [28-31]. On the other hand, the shift of the bands at 555 (535) cm^{-1} and 850 (808) cm^{-1} to lower wavelengths as well as the disappearance of the band at 910 cm^{-1}, in $TiO_{2\text{-}D}$, are correlated to the interaction between Mn and Ti and thus weakening Ti–O bonds.

The spectrum of $TiO_{2\text{-}SG}$ shows bands characteristic of anatase (500, 532, 610 cm^{-1}) and rutile (460 cm^{-1}) indicative of vibration modes of titanium oxide structure, O–Ti–O [27]. Mn incorporation by sol–gel with titania ($Mn/TiO_{2\text{-}SG}$) indicated the same bands devoted for the latter sample ($TiO_{2\text{-}SG}$) with exhibiting shifts to higher wavenumbers [(480 (460), 513 (500), 554 (532) and 616 (610)] pointing to the strong interaction between Mn and Ti moieties. The appearance of new bands at 655 and 693 cm^{-1} not present in $TiO_{2\text{-}SG}$ is probably due to vibration of

β-MnO_2, which assumes a tetragonal structure [28,32]. Thus, an expected cation exchange can be assumed, in the sense that Ti and Mn ions have similar ionic radii. This can be emphasized from lattice parameter c value of $Mn/TiO_{2\text{-SG}}$ that showed a decrease compared with $TiO_{2\text{-SG}}$ based on displacement of some Ti atoms from their sites. Accordingly, Mn^{4+} may partially incorporated into the titania network [Mn^{4+} (0.60 Å) than Ti^{4+} (0.68 Å)] influencing their crystals size. Therefore, during the impregnation and sol–gel procedures the Mn(IV) and Mn(III) can be located in the octahedral positions substituting Ti ions [33].

On the other hand, the IR spectrum of OH groups in the parent $TiO_{2\text{-D}}$ shows bands at 3736, 3715_{sh}, 3676 and 3663 cm^{-1} assigned, respectively, to surface isolated hydroxyl groups; which are located on TiO_2 of different crystallographic planes [34,35] and bridging $(TiO)_2OH$ groups [36]. Mn incorporation results in increase of the bands intensity of the free OH groups of $TiO_{2\text{-D}}$ with a marked increase in wavenumbers; such as 3736 (to 3752 cm^{-1}) and 3676 (to 3684 cm^{-1}), together with vanishing those at 3715 and 3676 cm^{-1} pointing that Mn are localized on them. Simultaneously, a new band at 3630 cm^{-1} in $Mn/TiO_{2\text{-imp}}$ indicative of hydrogen bonded OH groups and represents acidic hydroxyls is obtained.

The TiO_2 sample prepared by sol–gel shows bands at 3744, 3694 and 3650 cm^{-1} comparable to those exhibited by $TiO_{2\text{-D}}$ (3735, 3676 and 3663) but of lower intensities. The band at 3744 cm^{-1} is shifted to higher wavenumbers to 3768 cm^{-1} when Mn introduced into titania indicating that the inclusion of Mn enhances the number (increasing the band intensity) and strength (shift towards higher wavenumber) of this particular free OH group. The same behavior was also depicted for the 3694 (3689) cm^{-1} band except that non significant shift in wavenumber. The hydrogen bonded OH groups occurred at 3637 cm^{-1} in $Mn/TiO_{2\text{-SG}}$ was significantly decreased in intensity when compared with that at 3650 cm^{-1}; in $TiO_{2\text{-D}}$, implying the increase of protonic nature of the former than that of the latter [37] and hence Bronsted acidity. Whereas, the band at 3630 cm^{-1} in $Mn/TiO_{2\text{-Dimp}}$ was more acidic than that of $Mn/TiO_{2\text{-SG}}$ at 3637 cm^{-1} and of high populations.

3.4. Catalytic activity

The zeta potential profile of $Mn\text{-}TiO_{2\text{D-imp}}$ suspension is shown in Fig. 5; as an example. This Figure shows that the zero point charge is at 4 that was comparable to that of MnO_x species [38]. Hence, the oxidizing ability of MnO_x can sharply be enhanced [39] at pH values lower than 4 since MnO_x surfaces will acquire positively charges below this pH based on their ZPC. This value shows that ca. 34% of the support titania; that has ZPC around 6.1, is covered by Mn species, i.e. surface coverage. IC is a dianionic dye in aqueous solution and it can keep its dianionic configuration in the pH range 2–11 [17]. At low pH range, electrostatic interactions between the positive catalyst surface and dye anions lead to strong adsorption of the latter on the metal oxide support. On the other hand, Mn/TiO_{2SG} indicates ZPC at 5.5 (not shown) reflecting a decrease in the amount

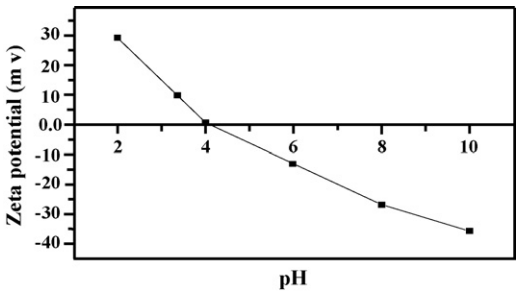

Fig. 5. The time-resolved absorption spectra during the reaction of 100 ppm of IC in the presence of 100 mg $Mn/TiO_{2\text{-Dimp}}$ catalyst under UV illumination. Decreasing absorbance of the bands for IC is related to 2, 4, 8, 12, 16, 25, 45 min from up to down.

of Mn covered the surface to ∼10%. This result indicates that the majority of Mn ions exchanges titania in its lattice structure. This was in agreement with the results obtained from IR and lattice parameters.

Fig. 6 shows the UV–vis absorption spectra of the IC dye solutions irradiated by UV light in the presence of $Mn/TiO_{2\text{-Dimp}}$ catalyst. IC itself in the absence of a catalyst was photochemically inert (blank) as pointed out by no change in the absorption spectrum. The maximum wavelength for IC dye was determined to be 608 nm. This peak accounts for the blue color of solutions and can be attributed to the $n \rightarrow \pi$ (transition of the non-bonding electrons to the anti-banding π) group orbital of the double bond system and it is used to monitor the mineralization of the dye [32]. In the UV region (not well shown due to limitation of the apparatus), there is a second group of bands characteristic of aromatic rings. The position of the maximum absorption (608 nm) was significantly varied and gradually shifted to lower wavelengths (575 nm) till disappearing. Increasing the mineralization efficiency of IC on $Mn/TiO_{2\text{-Dimp}}$ is accounted for oxidative degradation of the dye. The peak appeared at 330 nm characteristics of photoreduction products is shifted to lower wavelengths lower than 300 nm indicative of aromatic rings destruction.

The calculated amount of CO_2 evolved from the reaction that was captured by an aqueous solution of barium hydroxide and determined gravimetrically as precipitated barium carbonate measured 55% of the dye carbon atoms calculated theoretically. The sulphate ions, on the other hand, determined as barium

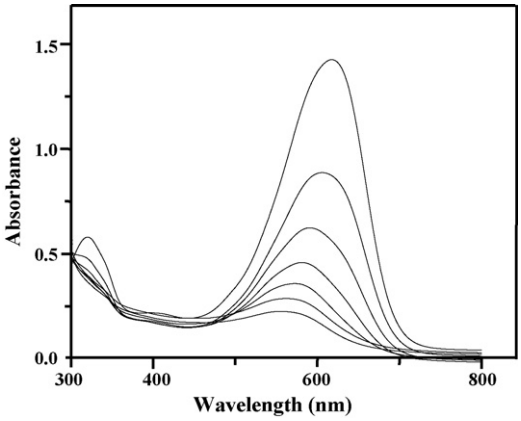

Fig. 6. Zeta potential of IC on $Mn/TiO_{2\text{-Dimp}}$ as a function of solution pH.

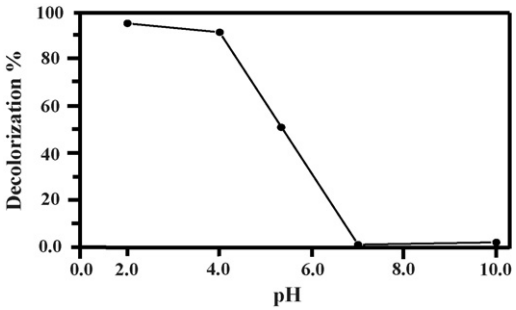

Fig. 7. Effect of pH on the decolorization percentages of IC on $Mn/TiO_{2\text{-}Dimp}$. *Experimental conditions*: reaction volume 300 ml, catalyst content 100 mg, reaction time 60 min, initial dye conc. 100 ppm.

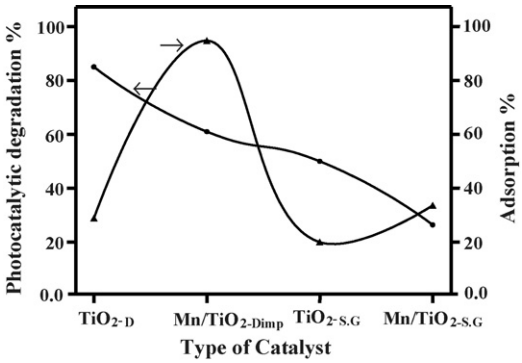

Fig. 8. The efficiency of IC decolorization (adsorption) and photodegradation over various catalysts. *Experimental conditions*: pH 2, reaction volume 300 ml, catalyst content 100 mg, reaction time 60 min, initial dye conc. 100 ppm.

sulphate using barium chloride solution measured lower value than that expected based on stoichiometric ratios possibly due to the adsorption of some sulphate ions on the catalyst surface. These results indicate that oxidative degradation of IC on $Mn/TiO_{2\text{-}Dimp}$ is proposed. This may be described involving the diffusion of the dye to the particle surface forming a complex, followed by exchange of electrons with the active sites on the surface [31]. As a hydrophilic substrate, IC may easily diffuse to and accumulate at the surface of the catalyst active sites facilitated by the decreased pH of the reaction mixture that was at 2. Thus, one can postulate that the electrostatic attraction between the protonated dye molecules and $Mn_2O_2H_2^+$ moieties can takes place in this pH range [38].

3.4.1. Effect of pH on the adsorption of IC

The adsorption efficiency of IC on $Mn/TiO_{2\text{-}Dimp}$ at different pH levels was shown in Fig. 7. The pH of the solution was adjusted with dilute NaOH and HCl solutions. It was found that the decolorization of the dye over $Mn/TiO_{2\text{-}Dimp}$ was highly pH dependent reaching maximum removal (98%) at pH 2. At pH > 10, the decolorization of the dye was negligible. Both the surface charge of Mn/TiO_2 and the solution speciation of IC changed with pH. The possible explanation of that behavior is that as the initial pH of dye solution decreases, the catalyst presents a positive charge thus promoting the adsorption of dye since it contains negative sulfonate groups [31].

Accordingly, the dependence of photocatalytic mineralization on pH is expected to rely on different reaction mechanisms such as hydroxyl radicals attack, direct oxidation by positive hole and direct reduction by the electron in the conducting band those can contribute to dye mineralization. The importance of each one depends on dye nature and pH [40]. In this study, pH 2 was found to be the optimal pH under the given experimental conditions. Reduction by electrons in conduction band may play a very important role in the mineralization of dyes due to reductive cleavage of azo bonds. In addition, Mn/TiO_2 particles tend to agglomerate under acidic condition [7,31] and the surface area available for dye adsorption and photon absorption would be reduced. An additional explanation for the pH effects can be related with changes in the specification of the dye. That is, protonation or deprotonation of the dye can change its adsorption characteristics and redox activity [41]. For IC molecules at lower pH, strong Coulombic attraction onto photocatalyst takes place where this is not the case at high pH values due to repulsive electrostatic forces.

3.4.2. Comparison between photocatalysis and adsorption of materials

The decolorization efficiency of IC on $TiO_{2\text{-}D}$, $Mn/TiO_{2D\text{-}imp}$, $TiO_{2\text{-}SG}$ and $Mn/TiO_{2\text{-}SG}$ in the absence (adsorption) or presence of ultraviolet irradiation at pH 2 was shown in Fig. 8. This figure shows that the removal activity (adsorption) in the absence of ultraviolet decreased in the order; $TiO_{2\text{-}D}$ (88%) > $Mn/TiO_{2D\text{-}imp}$ (60) > TiO_{2SG} (50%) > $Mn/TiO_{2\text{-}SG}$ (28%). Increasing the removal activity of $TiO_{2\text{-}D}$ than $TiO_{2\text{-}SG}$ may be due to increasing the population of surface hydroxyls of this particular sample. This high surface concentration, as confirmed by FTIR results, is supported by the fact that the large extent of the anatase phases (100%); even though calcined at 550 °C, was responsible for enriching with surface hydroxyls. In addition to the large surface to volume ratio the $TiO_{2\text{-}D}$ nanoparticles has. Consequently, this kind of interaction takes place inside the catalyst internal surface; rather than external ones, since the former represents more than 90% of total surface area. This was highly emphasized based on knowing the molecular size of IC dye ($1.55 \times 0.64 \times 0.41$ nm) [42] thus suggesting its free diffusion inside the pores of $TiO_{2\text{-}D}$ (3.3 nm). This increased adsorption capacity of $TiO_{2\text{-}D}$ is also strongly related to the binding sites composed of two groups of sulfonate with hydroxyl groups of titania; those regarded as adsorptive sites for compounds tending to form hydrogen bonding.

The observed higher rate of photocatalytic mineralization of IC dye on $Mn/TiO_{2D\text{-}imp}$ is found to be 3.5 times as high as those on $TiO_{2\text{-}D}$. This is probably correlated to the role played by exposed Mn species on the surface of titania in speeding up the activity of the photocatalyst by releasing electrons and holes (O^- lattice and/or $^*OH$ radicals) under illumination. The photogenerated e^-/h^+ pairs can easily and quickly diffuse to the surface of catalysts to form active sites at which photocatalytic (redox) reactions are produced. More specifically, in Mn loaded TiO_2, the photogenerated electrons transfer from TiO_2 to Mn particles and the holes remain on the TiO_2, resulting in charge separation of the photo-formed e^-/h^+ pairs with good efficiency, as confirmed for Pt loaded TiO_2 [43]. In addition,

the oxidation–reduction capabilities of this particular catalyst is much dependent on exposing Mn^{3+} moieties on the titania surface; as revealed by FTIR results. However, in $TiO_{2\text{-}D}$ particle crystallinity strongly influence the recombination rate of e^-/h^+ [44]. Surprisingly, both TiO_{2SG} and Mn/TiO_{2SG} catalysts presented lower activity either in adsorption or in photocatalysis as they compared to $Mn/TiO_{2D\text{-}imp}$ although former catalysts exhibited smaller nanoparticles than those in the latter. This could nullify the effect of particles size since they have comparable values in the 43–48 nm range. The decreased activity of Mn/TiO_{2SG} in both adsorption and photo-mineralization is accounted for the alteration in bulk electronic structure; depending on that major amount of Mn ions are probably incorporated in the titania lattice influencing their light absorption and consequently the electron-hole generation and separation capacity, i.e. the insertion of manganese ions; as MnO_2, in the TiO_2 lattice decreases the ability of the TiO_2 to produce hole and electrons and inhibit the evolution of Mn^{4+}-Mn^{3+} moieties upon irradiation.

On the other hand, although $TiO_{2\text{-}SG}$ presented appreciable absorption capacity (50%), it shows the lowest photo-mineralization activity (20%) between all samples. This could be correlated to fast recombination of e^-/h^+ in this sample. This clarifies that the smaller size may not be good for the e^-/h^+ separation necessary for efficient photocatalytic degradation [45]. The absence of synergetic effect of anatase-rutile mixed phase in TiO_{2SG} and Mn/TiO_{2SG} catalysts may depend on bad contacted interfaces between the two phases [46], i.e. unsuccessful e^- transfer from rutile to anatase is responsible for decreasing the charge separation and accordingly decreases the photo-catalytic reaction at the particle surfaces.

3.4.3. Effect of time

It can be seen that the dye removal process on $Mn/TiO_{2D\text{-}imp}$ was found to proceed through two stages. An initial rapid phase for the first 5 min that was found to compromise 40% adsorption as shown in Fig. 9. Another stage extends to 30 min exhibiting 86% removal. The dye removal thereafter attains saturation in 40–70 min and finally increases to reach 100% adsorption (removal) in 70 min reaction time. The higher sorption rate at the initial period (5 min) may be due to an increased number of vacant sites available at the initial stage and as a result an expected variation in the concentration of adsorbate in solution and on adsorbent surface (concentration gradient) tends to enhance the dye sorption rate at initial stages. As time proceeds, this concentration gradient decreases due to accumulation of dye molecules on vacant sites and thus a virtually saturation stage was perceived.

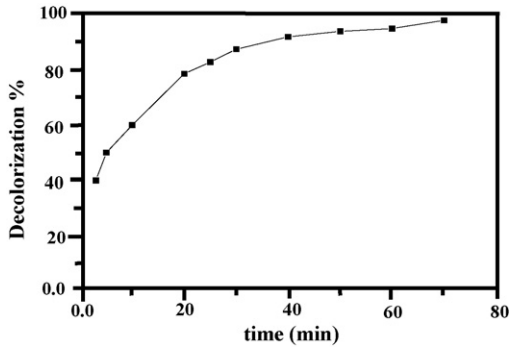

Fig. 9. Kinetics of IC adsorption on $Mn/TiO_{2\text{-}Dimp}$. *Experimental conditions*: pH 2, $T = 25\,^{\circ}C$, catalyst mass = 100 mg, volume = 300 ml, initial dye conc. 100 ppm.

4. Conclusion

Manganese supported on titania synthesized by impregnation method showed the highest photocatalytic activity for effective mineralization of IC dye. This apparent activity can be due to:

(1) The involvement of Mn^{3+} moieties as Mn_2O_3 in TiO_2 ($Mn/TiO_{2D\text{-}imp}$) was responsible for improving electronic and thus optical properties of such nanometer sized particles. Conversely, Mn/TiO_{2SG} exhibited strong shift to high wavenumbers due to involvement of β-MnO_2 in the lattice structure of TiO_2 thus presuming partial incorporation of Mn into titania lattice and as a result influencing oxidation–reduction capabilities.
(2) Zeta potential measurements estimated that ca. 34% of titania support is covered by Mn in $Mn/TiO_{2D\text{-}imp}$ where on Mn/TiO_{2SG} only 10% of Mn covered the surface of titania revolving the lower ability of the latter to absorb light to effectively degrade the dye.
(3) Strengthening acidic hydroxyls specifically those located at 3630 cm^{-1} in $Mn/TiO_{2D\text{-}imp}$ than those at 3637 cm^{-1} in Mn/TiO_{2SG} of lower population was responsible for lowering the activity of the latter than that of the former.

The adsorption of IC on $TiO_{2\text{-}D}$ was considerably higher than all catalysts and well regulated by pH. This was due to increasing the population of OH groups, high surface to volume ratio and the facile diffusion of IC onto the catalyst particle followed by its allocation into internal surfaces.

References

[1] M.S. Chiou, H.Y. Li, Chemosphere 50 (2003) 1095.
[2] M.S. Chiou, H.Y. Li, J. Hazard. Mater. 93 (2002) 233.
[3] A. Verberckmoes, B.M. Weckhuysen, R.A. Schoonheydt, Micropor. Mesopor. Mater. 22 (1998) 165.
[4] J.B. Yin, X.P. Zhou, Chem. Mater. 14 (2002) 4633.
[5] Y. Komoda, N. Sakai, T.N. Rao, Langmuir 14 (1998) 1081.
[6] R. Arroyo, G. Cordoba, J. Padilla, V.H. Lara, Mater. Lett. 54 (2002) 397.
[7] A.K.H. Nohman, M.M. Mohamed, M.I. Zaki, Curr. Top. Catal. 4 (2005) 45.
[8] A.T. Stone, J.J. Morgan, Environ. Sci. Technol. 18 (1984) 617.
[9] W.G. Sunda, D.J. Kieber, Nature 367 (1994) 62.
[10] R. Liu, H. Tang, Wat. Res. 34 (2000) 4029.
[11] T.D. Waite, I. Wrgley, R. Szymczak, Environ. Sci. Technol. 22 (1988) 778.
[12] G. Qi, R.T. Yang, Appl. Catal. B 44 (2003) 217.
[13] A. Chen, H. Xu, Y. Yue, W. Hua, W. Shen, Z. Gao, J. Mol. Catal. A 203 (2003) 299.
[14] D.A. Pera, B.S. Uhade, P.G. Smirniotis, J. Catal. 221 (2004) 421.
[15] F.J. Green (Ed.), The Sigma Aldrich Handbook of Stains, Dyes and Indicators Aldrich Chemical, Milwaukee, WI, 1990, p. 403.
[16] M. Vautier, C. Guillard, J.M. Hermann, J. Catal. 201 (2001) 46.

[17] C. Galindo, P. Jacques, A. Kalt, J. Photochem. Photobiol. A. 141 (2001) 47.
[18] J.A. Kettle, B.M. Clark, C.C. Winterbourn, J. Biol. Chem. 279 (2004) 18521.
[19] C. Flox, S. Ammar, C. Arias, E. Brillas, A.V. Vergas-Zavala, R. Abdelhedi, Appl. Catal. B 67 (2006) 93.
[20] G. Pecchi, P. Reyes, L. Lopez, R. Gomez, A. Moreno, J.L.G. Fierro, J. Chem. Tech. Biotech. 77 (2002) 144.
[21] B.O. Hincapie, L.J. Garces, Q. Zhang, A. Sacco, S.L. Suib, Micropor. Mesopor. Mater. 67 (2004) 19.
[22] J.I. Langford, J.C. Wilson, J. Appl. Cryst. 11 (1978) 102.
[23] L. Azaroff, M. Buerger, The Powder Method in X-ray Crystallography, Mc Graw-Hill, New York, 1958, p. 254.
[24] A.M. Tonejc, I. Djerdj, A. Tonejc, Mater. Sci. Eng. C 19 (2002) 85.
[25] M.M. Mohamed, Appl. Catal. A 267 (2004) 135.
[26] X.T. Yoko, K. Kamiya, K. Tanaka, J. Mater. Sci. 25 (1990) 3922.
[27] J. Zhang, I. Boyd, B.J.O. Sullivan, P.K. Hurley, P.V. Kelly, J.P. Senateur, J. Non-Cryst. Solid 303 (2002) 134.
[28] M.I. Zaki, M.A. Hasan, L. Pasupulety, K. Kumari, Thermochim. Acta 303 (1997) 171.
[29] F.A. Al-Sogheer, M.I. Zaki, Micropor. Mesopor. Mater. 67 (2004) 43.
[30] M.M. Mohamed, J. Colloid. Inter. Sci. 272 (2004) 28.
[31] I. Othman, R.M. Mohamed, I.A. Ibrahim, M.M. Mohamed, Appl. Catal. A 299 (2006) 95.
[32] R.M. Potter, G.R. Rossman, Am. Miner. 64 (1979) 1199.
[33] Y.H. Hu, E. Ruckenstein, J. Catal. 158 (1996) 260.
[34] A. Yamakata, T. aki Ishibashi, H. Onishi, Bull. Chem. Soc. Jpn. 75 (2002) 1019.
[35] P. Jackson nd, G.D. Parfitt, Trans. Faraday Soc. 67 (1971) 2469.
[36] M.M. Mohamed, W.A. Bayoumy, M. Khairy, M.A. Mousa, Micropor. Mesopor. Mater. 97 (1–3) (2006) 66.
[37] M. primet, P. Pichat, M. Michel-Vital, J. Phys. Chem. 75 (1971) 1216.
[38] P. Mulvaney, L. Denison, F. Grieser, R. Cooper, J.V. Sanders, D. Meisel, J. Colloid. Interf. Sci. 121 (1988) 71.
[39] A.T. Stone, Environ. Sci. Tech. 21 (1987) 979.
[40] M.H. Habibi, A. Hassanzadah, S. Mahdavi, J. Photochem. Photobiol. A 172 (2005) 89.
[41] I.K. Konstantinou, T.A. Albanis, Appl. Catal. B 49 (2004) 1.
[42] S. Ismadji, S.K. Bhatia, Langmuir 16 (2002) 9303.
[43] M. Anpo, M. Takenchi, J. Catal. 216 (2003) 505.
[44] J. Villasenor, P. Reyes, G. Pecchi, Catal. Today 76 (2002) 121.
[45] R.K. Wahi, W.W. Yu, Y. Liu, M.L. Mejia, J.C. Falkner, W. Nolte, V.L. Colvin, J. Mol. Catal. A 242 (2005) 48.
[46] N.M. Mahmoodi, M. Arami, N.Y. Limaee, N.S. Tabrizi, Chem. Eng. J. 112 (2005) 191.